LANGMUIR

pubs.acs.org/Langmuir
Article

Binding Modes and Water-Mediation of Polyelectrolyte Adsorption to a Neutral $CaCO_3$ Surface

Alec Glisman, Sriteja Mantha, Decai Yu, Eric Paul Wasserman, Scott Backer, Larisa Reyes, and Zhen-Gang Wang*

Cite This: *Langmuir* 2024, 40, 25931−25939
Read Online

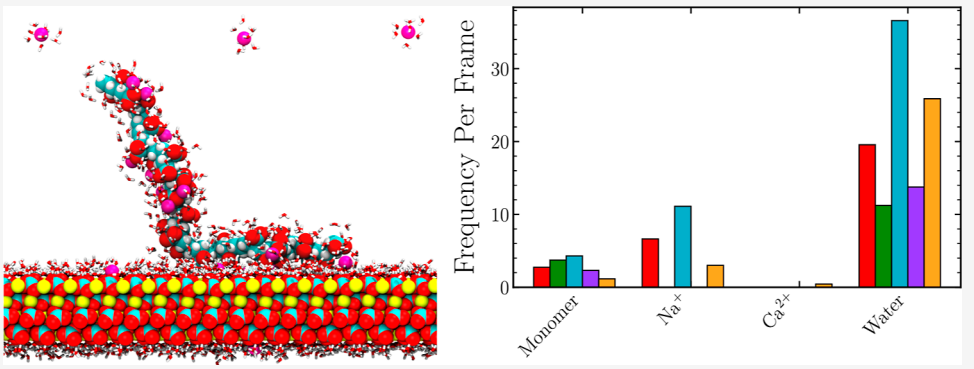

ABSTRACT: Aqueous polyelectrolytes are effective mineralization inhibitors due to their ability to template onto crystal surfaces and chelate ions in solution. These additives have been shown to alter the morphology of calcium carbonate crystals, making them promising candidates for biological and industrial applications. However, while key to designing more effective mineralization inhibitors, the molecular mechanisms governing the interactions between polyelectrolytes and crystal surfaces remain poorly understood. In this study, we investigate the adsorption of poly(acrylic acid) (PAA) on the dominant calcite $(10\bar{1}4)$ cleavage plane using all-atom molecular dynamics simulations. Although the calcite slab is electrostatically neutral, its charge distribution induces a strong electrostatic potential in an aqueous solution, which leads to significant water structuring at the interface. We observe a very favorable adsorption affinity of the polyelectrolyte chain to the surface, yet the structure of the interfacial water is not significantly affected. Direct interactions between the monomers on the polyelectrolyte and the calcite surface are infrequent, despite variations in chain length, charge density of the polyelectrolyte, and solution conditions. Intriguingly, the polyelectrolyte interaction with the calcite surface is dominantly mediated through bridging hydrogen bond interactions. As the polyelectrolyte adsorbs to the surface, the chain conformation adapts to the interfacial water structure by increasing polyelectrolyte−water contacts and integrates into pre-existing hydrogen bond networks. We found that water-mediated interactions are more dominant than direct interactions between the polyelectrolyte and the surface. This suggests an alternative pathway to the widely accepted notion that entropic effects due to water reorganization are the primary driving force. These results suggest that the polyelectrolyte binding affinity can be tuned by altering the polymer chain interactions with the interfacial water structure in addition to the surface itself.

INTRODUCTION

The process of mineralization or the formation of solid mineral deposits is ubiquitous in nature and in industry. In biological systems, mineralization is essential for the formation and growth of bones, teeth, and shells.[1−3] For example, sea shells are composed of calcium carbonate ($CaCO_3$) crystals, which form through the precipitation of Ca^{2+} and CO_3^{2-} ions from seawater and exhibit highly ordered structures.[4] Interestingly, the common polymorph of $CaCO_3$ in sea shells is aragonite, which is metastable relative to the thermodynamically stable calcite polymorph. It is believed that the formation of aragonite is influenced by the presence of small ions[5,6] and macromolecules such as proteins and polyelectrolytes (PE).[7−9]

However, mineralization can also be detrimental, forming scale deposits in industrial processes, such as in water treatment facilities and desalination plants.[10,11] In addition to polymorph and morphology control, industrial processes require the inhibition of mineralization to prevent scale formation or limit the growth of pre-existing mineral deposits.

Received: August 22, 2024
Revised: November 4, 2024
Accepted: November 19, 2024
Published: December 2, 2024

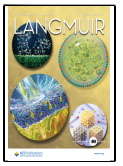

For both of these applications, aqueous solutions of PEs, such as poly(acrylic acid) (PAA), have shown promise as an effective means of controlling mineralization.

PEs are particularly effective at inhibiting $CaCO_3$ growth due to their ability to chelate Ca^{2+} ions and modify or slow crystal growth through their charged functional groups.[12−17] PEs have also been shown to stabilize amorphous calcium carbonate,[18,19] stabilize the vaterite polymorph,[20] and alter the surface morphology of $CaCO_3$ precipitates.[21,22] While the effects of PEs on $CaCO_3$ growth have been well-documented, the molecular mechanisms underlying the growth modification and inhibition of $CaCO_3$ by PEs are poorly understood. It is believed that PEs can template the growth of $CaCO_3$ crystals by preferential binding patterns and by altering the local environment around the growing crystal,[13] but the specific interactions between PEs and $CaCO_3$ surfaces are not well characterized.

Many research efforts have employed molecular modeling to describe the crystalline phase of $CaCO_3$ as well as its interfaces with water and organic molecules.[23−31] Aschauer et al.[29] used molecular dynamics (MD) simulations to investigate the growth modification of calcite with a step defect by PAA with a chain length of 10 monomers. They found that the adsorption of PAA on the calcite surface was energetically unfavorable but was stabilized by an increase in the system entropy due to the destruction of the interfacial water structure. PAA was seen to weakly bind to the step defect and decrease the translational and orientational order of water molecules at the interface. Sparks et al.[30] built on this work by investigating the adsorption of longer PAA chains (28 monomers) on the calcite $(10\bar{1}4)$ surface. It was found that the longer PAA chains preferentially adsorbed with an extended conformation parallel to the calcite surface and that only a small fraction of the PAA chain was adsorbed on the surface. In neither study did the authors observe multiple binding events in a single trajectory of 1−2 ns. The limited ensemble sampling suggests that longer simulation times are needed to observe the full range of binding modes.

Previous MD studies on biomolecular binding to $CaCO_3$ surfaces have highlighted the critical role of water-mediated hydrogen bonding between the crystalline surface and biomolecules in facilitating binding interactions.[32,33] Zhu et al.[31] showed that water molecules near calcite surfaces exhibit strong positional and orientational ordering, and this ordering significantly affects the adsorption of AA dimers. We aim to build upon these results by quantifying the relative contributions of water mediation, ionic mediation, and direct interactions between the binding PAA chain and the crystalline surface.

Our previous work investigated how PEs can chelate Ca^{2+} ions to prevent nucleation of $CaCO_3$ crystal, as well as precipitate PE−ion complexes.[34,35] In this study, we extend our previous models to investigate the adsorption of PAA on a $CaCO_3$ surface. We aim to elucidate the molecular mechanisms that govern the adsorption of PAA on a $CaCO_3$ surface to understand what design principles may lead to more effective antiscalant PEs. We focus on the adsorption of a model PE PAA on the calcite $(10\bar{1}4)$ surface, the dominant cleavage surface of calcite in aqueous solution.[36] We sought to probe the effects of chain length, PE charge density, and aqueous solution conditions on the adsorption behavior of PAA on the calcite surface, with a particular focus on the role of water in mediating the adsorption process.

The rest of the article is organized as follows. In the Methods section, we describe the model and parameters used in our enhanced sampling of MD simulations. We then present the results of our study and discuss the implications of our findings in the Results and Discussion section. Finally, we summarize our findings and suggest future research directions in the Conclusions section.

METHODS

We studied the adsorption properties of PAA on the calcite $(10\bar{1}4)$ surface using MD simulations. Six systems were simulated, as shown in Table 1. The $(10\bar{1}4)$ surface was chosen as it is the most stable surface of calcite in water.[36] The systems included polymers with chain lengths of 16 and 32 monomers in both fully charged (PAA) and neutral (PAAn) forms. We also simulated a neat system with no added PE or aqueous ions to study the water−calcite interface as a comparison. While we aim to model systems under basic conditions (pH ∼ 9−11) under which PAA (with a pK_a of ∼4.5) should be completely ionized, we include the neutral form of the acrylic acid monomer AAn in order to examine the effects of charge without introducing additional interaction effects. These neutral AAn monomers can also be considered as an approximate proxy for other neutral monomers in acrylic copolymers. In addition, PAAn, to a first approximation, also serves as a proxy for other neutral antiscalant polymers, such as vinyl alcohol-based variants, and to provide adsorption behavior in the absence of charge. For systems with charged monomers, Na^+ ions were added to neutralize the system. The 32-mer PAA system was also simulated with 32 Ca^{2+} ions to investigate the effect of aqueous multivalent ions on adsorption behavior.

Table 1. Polyelectrolyte and Ion Systems Simulated for Single-Chain Adsorption on the Calcite $(10\bar{1}4)$ Surface[a]

polymer	aqueous ions	box length (nm)
neat (no PE)		9
16-PAA	16 Na^+	9
16-PAAn		9
32-PAA	32 Na^+	12
32-PAAn		12
32-PAA	32 Na^+, 32 $CaCl_2$	12

[a]The polymer entries indicate the number of monomers in the polymer chain and whether they are charged (AA) or neutral (AAn) acrylic acid monomers. The ions indicate the number of ions in the system, and the box length indicates the linear dimension of the simulation box in the x and y directions. The z direction is perpendicular to the calcite surface and is 1 nm longer than the box length to accommodate the approximately 1 nm thick calcite slab.

The initial polymer structures were generated using CHARMM-GUI[37,38] with atactic stereochemistry. Calcite crystal structures were taken from the American Mineralogist Crystal Structure Database[39] with data from Markgraf and Reeder.[40] Following previous work,[28] the unit cell of the calcite slab was then sliced along the $(10\bar{1}4)$ plane to create a 1 nm thick slab in the z axis and replicated in the x and y axes to generate a supercell of the desired size using the Python Materials Genomics (PyMatGen) package.[41] Finally, the system was solvated with water molecules and neutralized with Na^+ ions using GROMACS tools[42−44] in an orthorhombic box with periodic boundary conditions. Snapshots of the systems after equilibration are shown in Figure 1.

Following the protocols and models established in our previous work,[34,35] we employed the SPC/E[45] water model and the general AMBER force field[46−48] to model the polymer chains as well as the calcite slab. To appropriately balance the strength of electrostatic interaction, we used the electronic continuum correction method[49,50]

https://doi.org/10.1021/acs.langmuir.4c03301
Langmuir 2024, 40, 25931−25939

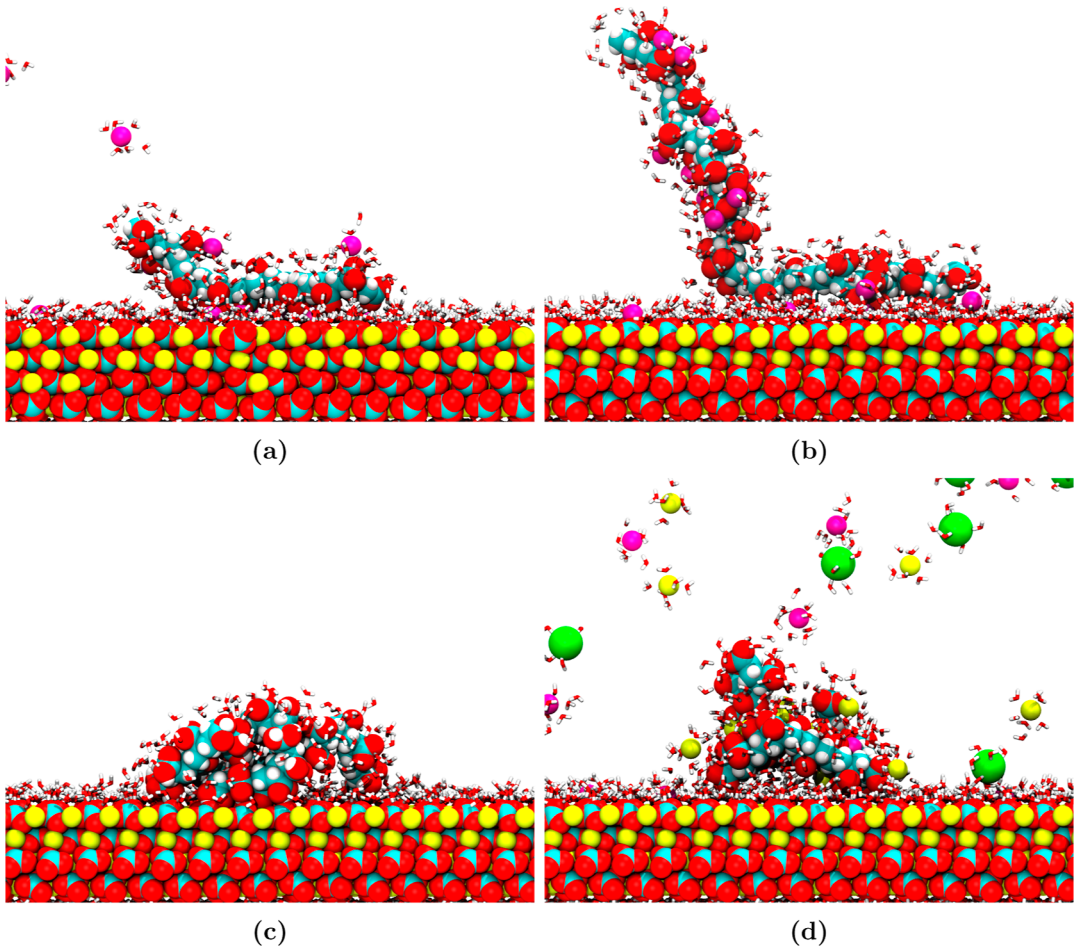

Figure 1. Snapshots of the polyelectrolyte binding to the calcite surface: (a) 16-PAA, (b) 32-PAA, (c) 32-PAAn, and (d) 32-PAA with 32 $CaCl_2$. The first solvation shell water molecules are shown in the licorice representation, and other atoms are shown in the van der Waals representation. Oxygen atoms are red, carbon atoms are gray, calcium atoms are yellow, sodium atoms are purple, chlorine atoms are green, and hydrogen atoms are white.

to correct the partial charges of all nonwater atoms in the system. Further details on the methodology can be found in Mantha et al.[34]

We used the GROMACS (version 2023.2) simulation package[42−44] patched with the PLUMED (version 2.9.0) plugin.[51−53] A cutoff distance of 1.2 nm was used for the van der Waals interactions, and the particle mesh Ewald method[54,55] was used to calculate the long-range electrostatic interactions with a real-space cutoff of 1.2 nm. The LINCS algorithm[56] was used to constrain the lengths of bonds involving hydrogen atoms, and the leapfrog algorithm was used to integrate Newton's equations of motion. Where applicable, the system temperature was maintained at 300 K using the Nosé−Hoover thermostat[57,58] with a 0.25 ps relaxation time constant. For *NPT* simulations, the pressure was maintained at 1 bar using the semi-isotropic Parrinello−Rahman barostat[59] with a 5.0 ps relaxation time constant. To mimic the near-incompressible nature of the crystalline slab, the compressibility was set to 4.5×10^{-5} bar^{-1} in the z direction and 4.5×10^{-15} bar^{-1} in the x and y directions to keep the interfacial area fixed such that the crystal lattice size would not fluctuate parallel to the surface.[60,61]

The systems were energy minimized using the steepest descent algorithm for approximately 100,000 steps. The systems were then equilibrated for 5 ns in the *NVT* ensemble, followed by 5 ns in the *NPT* ensemble with a time step of 1 fs to equilibrate the system temperature and density. Finally, production *NVT* simulations with a time step of 2 fs were run for 500 ns to converge the chain adsorption potential of the mean force (PMF). Harmonic restraints were applied to the calcite slab to prevent the slab motion during the simulations. The first 50 ns of each simulation were used for equilibration in the *NVT* simulation, and the remaining 450 ns were used for analysis.

The neat system—without aqueous ions or polymer—was simulated with traditional MD integration. However, to enhance the polymer conformational sampling, we used the on-the-fly probability-enhanced sampling (OPES) method developed by Invernizzi and Parrinello[62] and later extended to replica exchange (OneOPES) techniques by Rizzi et al.[63] The OneOPES method uses eight replicas with varying bias potentials to enhance the sampling of the polymer adsorption conformations and improve the convergence of the free energy calculations. The base (first) replica contains a single OPES bias potential, and the remaining replicas contain multiple OPES bias potentials with increasing strength, such that the highest (eighth) replica rapidly explores the entire free energy landscape. Exchange attempts are made between neighboring replicas every 1000 steps, and the enhanced sampling parameters were tuned to achieve a minimum average exchange acceptance rate of 20%.

In the first replica, the z distance between the center of mass of the polymer and the calcite surface was used as the collective variable (CV) for the OPES Explore bias potential.[64] The distance CV was updated with a 10,000 step pace, 0.2 nm width, and 30 kJ/mol barrier. The second replica added a second OPES Explore bias potential on the polymer radius of gyration with a 20,000 step pace, 0.02 nm width, and a barrier of 8 kJ/mol. The third replica added a third OPES Explore bias potential on the coordination number of aqueous ions around the carboxylate oxygens with a 20,000 step pace, 0.2 width, and 8 kJ/mol barrier. The coordination number was calculated with the continuous PLUMED coordination plugin with a switching

https://doi.org/10.1021/acs.langmuir.4c03301
Langmuir 2024, 40, 25931−25939

function of the form $s(r) = \frac{1-\left(\frac{r}{r_0}\right)^n}{1-\left(\frac{r}{r_0}\right)^m}$, where r is the pairwise distance between atoms with the following parameters: $n = 8$, $m = 16$, and $r_0 = 0.35$ nm. The fourth replica added a fourth OPES Explore bias potential on average z distance between the aqueous ions and the calcite surface with a 20,000 step pace, 0.2 nm width, and 8 kJ/mol barrier.

In addition to the OPES Explore bias potentials, the OneOPES method also uses the OPES MultiThermal bias potential[65] to allow the system to simultaneously explore multiple temperature distributions without altering the thermostat. The MultiThermal bias was updated with a 100 step pace and a maximum temperature of 304, 312, 326, 338, 354, and 374 K for replicas 3−8, respectively. Each replica contained independent OPES Explore and Multithermal bias potentials, as prescribed by the OneOPES method. Simulations of each polymer system condition consisted of five independent runs with different starting polymer conformations, and the results were averaged to obtain the final values. The error bars reported are 95% confidence intervals from independent simulations.

RESULTS AND DISCUSSION

The binding PMF for the PE chains is shown in Figure 2. The PMF is calculated as a function of the z distance from the chain center of mass to the top layer of the calcite surface (z_{surf}) such that $z_{surf} = 0$ corresponds to the upper layer of Ca^{2+} ions seen in Figure 1. Note that some carbonate oxygen atoms are located at $z_{surf} > 0$ due to rotation of the carbonate ions with respect to the calcite surface. Error bars are derived from the 95% confidence interval of five independent simulations. The reference state for each system is the free energy at $z_{surf} = 4$ nm, where the PE−calcite interaction has plateaued.

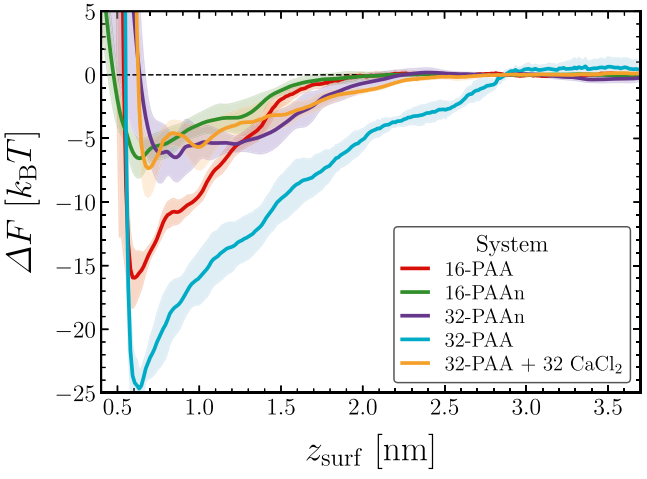

Figure 2. Potential of mean force for the z distance of the polymer chain center of mass from the calcite surface.

In all studied systems, the PE chains show a strong attraction to the calcite surface, as evidenced by the negative PMF values at short PE−surface distances ($z_{surf} < 1$ nm). The charged PEs (16-PAA/32-PAA) exhibit significantly stronger attraction to the calcite surface compared to the neutral polymers (16-PAAn/32-PAAn), indicating that electrostatic interactions between the PE and the calcite surface are the dominant driving force for adsorption. However, the PE−surface interaction appears to be mediated by other species as the PMF minimum occurs on average at distances of ∼0.65 nm.

The effects of chain length are also evident for the charged systems, with the PMF minimum shifting from 16 k_BT to 25 k_BT as the chain length increases from 16 to 32 monomers. The sublinear increase in binding affinity with chain length suggests that many PE monomers do not interact strongly with the calcite surface. As discussed in our previous work,[34,35] when aqueous Ca^{2+} ions are present, the PE chains strongly chelate the Ca^{2+} ions, thereby lowering the PE−ion complex charge density and reducing the electrostatic interactions with the calcite surface. The neutral systems also exhibit a weaker attraction to the calcite surface, consistent with their weaker electrostatic interactions. Additionally, the broader PMF minimum indicates that the adsorption binding modes are less specific and are more driven by solvent-mediated interactions.

To investigate how adsorption alters the PE chain conformation, we calculated the radius of gyration (R_g) of the PE chain as a function of the distance from the calcite surface (Figure 3). At short PE−surface distances, the PE chains exhibit an increase in R_g, as the chains extend toward the calcite surface to maximize the number of favorable interactions. The chain expansion occurs parallel to the calcite surface (see Figure S-1 in the Supporting Information) and is paired with a decrease in the chain size perpendicular to the surface due to the steric constraints of the calcite surface. Due to the chelation of aqueous Ca^{2+} ions, the 32 $CaCl_2$ system exhibits a much smaller R_g far from the surface than the salt-free system, which is consistent with Ca^{2+} ions facilitating intrachain ion bridges that reduce the chain's conformational freedom.[34] Ca^{2+} chelation in the 32 $CaCl_2$ system also causes PE expansion upon adsorption to be less favorable, which is consistent with the weaker adsorption observed. The neutral systems are more poorly solvated and exhibit a smaller R_g than the charged systems. While this size reduction minimizes PE−solvent interactions, it similarly minimizes the number of favorable PE−surface interactions, which may explain the weaker adsorption of the neutral systems.

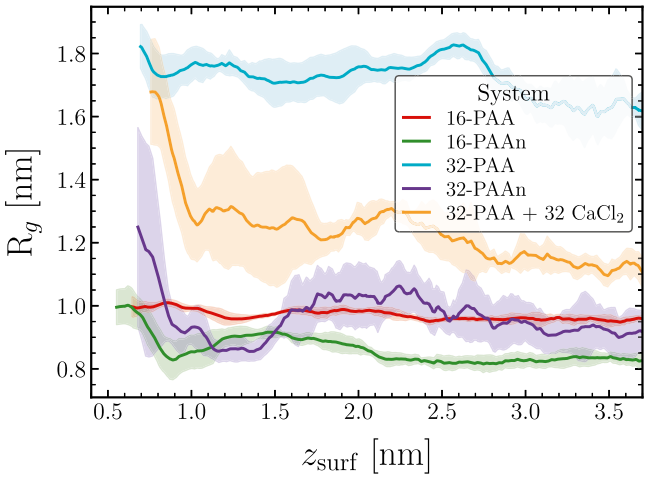

Figure 3. Polymer radius of gyration profile near the calcite surface.

We calculated the system electrostatic potential to understand the long-range and mediated electrostatic interactions between the PE chains and the calcite surface. The potential Ψ was calculated from Poisson's equation, $\nabla^2\Psi = -\rho_c/\epsilon_0$ with the system charge density ρ_c and vacuum permittivity ϵ_0. The potential profile was approximated as one-dimensional and solved using the average system charge density along the z-axis with periodic boundary conditions using a finite difference

https://doi.org/10.1021/acs.langmuir.4c03301
Langmuir 2024, 40, 25931−25939

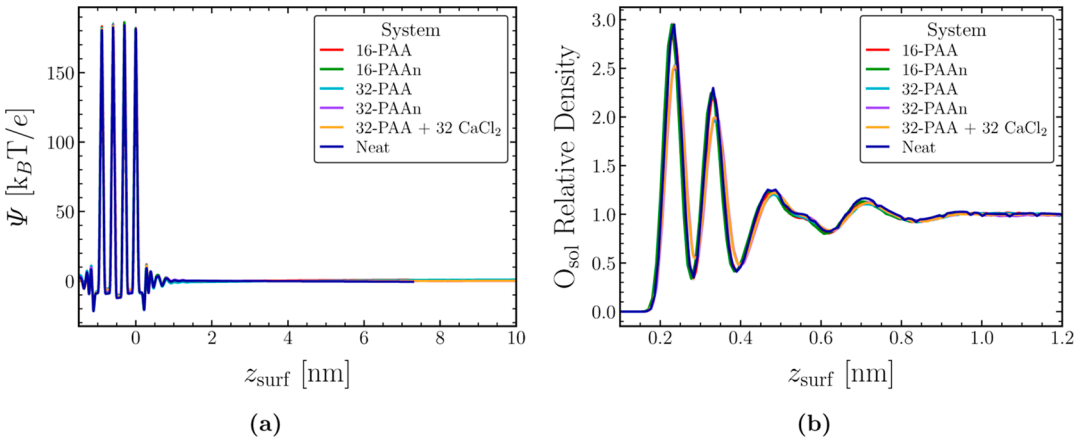

Figure 4. Average electrostatic potential profile of the system (a) and zoomed in near the calcite surface (b).

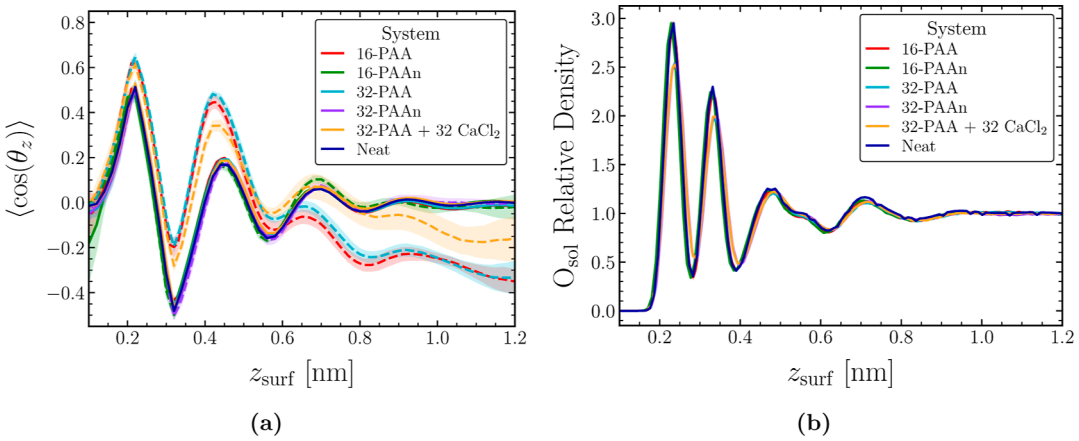

Figure 5. Interfacial water structure near the calcite surface. (a) Average water dipole moment angle profile of the PE solvation shell (dashed lines) and all water molecules (solid lines) near the calcite surface. The dipole moment angle is measured with respect to the +z axis such that $\cos(\theta) = 1$ indicates that the water oxygen is pointing directly toward the calcite surface and $\cos(\theta) = -1$ indicates that both water hydrogen atoms are pointing directly toward the calcite surface. The solvation shell is defined as all water molecules within 3.5 Å of the PE. (b) Solvent density (water oxygen) relative density profile near the calcite surface. The density is normalized by the bulk water density.

method. The electrostatically neutral calcite slab creates a highly negative potential near the surface due to the morphology of the calcite $(10\bar{1}4)$ surface (Figure 4b). As seen in Figure 1, the calcite layers consist of interleaved Ca^{2+} and CO_3^{2-} ions. The carbonate ions are oriented such that the oxygen atoms are pointing slightly outward from the surface, creating a charge distribution resulting in the potential profile shown in Figure 4a and inducing a strong dipole moment in the solvent near the calcite surface (Figure 5a).

The potential profile deviates significantly from the bulk potential, taken to be zero as a reference, in the interfacial region due to strong water structuring, as discussed below. A deep minimum in the potential profile is observed at the first water layer (~0.2 nm) as the water oxygen atoms are attracted to the positive potential inside the calcite slab. While the water structuring screens the electrostatic interactions, the potential fluctuations are on the order of 1 k_BT/e at distances of 1 nm. Notably, the potential profile is not significantly perturbed by the presence of PE chains or small ions. We hypothesize that this is likely due to the dilute concentrations of both the polymer chains and small ions under our solution conditions.

The potential profile near the calcite surface induces a strong dipole orientation of the solvent. In Figure 5a, we show the average water dipole moment angle of the solvent with respect to the +z axis. To highlight how the PE might alter the interfacial water orientational correlations, we plot the average water dipole moment angle of the PE solvation shell with dashed lines, whereas the average dipole moment angle of all water molecules is shown with solid lines. The electrostatic potential profile near the calcite surface is highly negative, which attracts the water hydrogen atoms toward the surface and repels the water oxygen atoms away from the surface, leading to a strong positive dipole moment for the first layer of water molecules. The second layer of water molecules is oriented so that the water oxygen atoms point toward the surface, facilitating hydrogen bonding with the first layer of water molecules.

Although the presence of PE does perturb the magnitude of the peaks/valleys in the dipole moment angle profile, the overall trend of the water molecules to orient according to the calcite surface is retained as the PE binds to the surface. This observation suggests that the PE does not significantly disrupt the water structure to maximize PE−surface interactions but instead modifies its structure to interact favorably with the interfacial water structure. At distances further from the surface, the influence of the calcite slab is weakened, and the PE solvation dominates the water structuring. This leads to a large difference between the water orientation of the solvation

https://doi.org/10.1021/acs.langmuir.4c03301
Langmuir 2024, 40, 25931−25939

shell and nonsolvating water molecules, as seen for $z \geq 1$ nm in Figure 5a. In addition to rotational ordering, water is translationally ordered near the calcite surface (Figure 5b) into two highly ordered and two weakly ordered layers. Note that the highly ordered layers are within 0.5 nm of the calcite surface, which is closer than the most favorable PE−surface distance of 0.65 nm. This indicates that PE dominantly adsorbs within the weakly ordered water layers and does not significantly perturb the highly ordered water layers directly adjacent to the calcite surface. The PE may displace water molecules from the interface as it binds, but this is a local rather than long-ranged effect. However, from Figure 5a, the structuring of the remaining interfacial water molecules does not appear to change significantly in the presence of the PE.

The dipolar correlations in Figure 5, coupled with the negative surface potential observed in Figure 4, can also influence small cations such as Na^+ and Ca^{2+} to accumulate near the calcite surface (see Figure S-2 in the Supporting Information). The adsorbed small ions can then facilitate the adsorption of the PE through ion bridges, which we have found to be important for bulk PE behavior.[34,35] In order to quantify the relative importance of these ion bridges as well as direct monomer adsorption and water-mediation, we plot the distribution of PE−calcite binding modes in Figure 6. It is

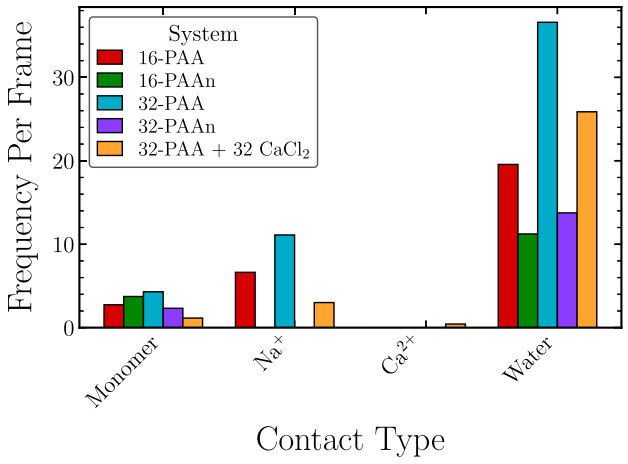

Figure 6. Distribution of binding modes of the PE to the calcite surface: direct monomer adsorption, Na^+ bridges, Ca^{2+} bridges, and water bridges. The *y*-axis is the average number of contacts formed between the PE and the calcite surface.

clear that direct monomer adsorption onto the calcite surface is not the dominant binding mode for the PE chains. On average, only 2−5 monomers are directly adsorbed to the calcite surface, with no clear trend related to chain length or charge density.

Instead, the dominant binding modes are Na^+ bridges (when Na^+ ions are present) and water bridges. A Na^+ bridge is defined as a Na^+ ion that is simultaneously coordinated to the PE and the calcite surface. The coordination exists when the Na^+ ion is within 3.5 Å of the PE and the calcite surface. Ca^{2+} bridges are defined similarly. Water bridges are defined as water molecules that simultaneously form hydrogen bonds with the PE and the calcite surface. These are the dominant binding modes for the PE chains with the number of water bridges increasing with chain length and charge density. Higher-order water bridges are also observed (see Figure S-3 in the Supporting Information), where multiple water molecules form a bridge between the PE and the calcite surface.

The 32 $CaCl_2$ system presents a unique case where the direct ion bridges between the PE and the surface are significantly reduced. The chelated Ca^{2+} ions commonly form intrachain ion bridges[34] and lower the number of carboxylate units available to form ion bridges with the surface. Additionally, the Ca^{2+} ion chelation reduces the number of water bridges as well as Na^+ bridges compared to the salt-free system, resulting in weaker adsorption of the PE chain to the calcite surface (Figure 2).

CONCLUSIONS

This study investigated the mechanisms driving the adsorption of PEs on crystalline surfaces. Specifically, we demonstrated that the adsorption of PAA on the calcite $(10\bar{1}4)$ surface is driven facilitated by the conformational changes of the PAA chains, which enable the polymer to integrate into the hydrogen bond network of the interfacial water layer. Although PE adsorption displaced some water molecules near the surface, the overall interfacial water structure remained largely unaffected.

Furthermore, the electrostatically neutral calcite slab generated a strong electrostatic field that ordered the interfacial water layers and attracted small ions to the surface. The resulting water-mediated and ion-bridging interactions dominated the PE−surface interactions. The first interfacial water layer at $z_{surf} \sim 0.20$ nm (Figure 5) appears to play a crucial role in the PE−calcite interactions. The PE fails to significantly penetrate the first water layer, as indicated by the low number of direct monomer contacts (Figure 6) and the most favorable interaction length scale of approximately 0.65 nm (Figure 2). Despite significant variations in chain length, PE charge density, and solution conditions affecting the binding affinity of the PE (Figure 2), the interfacial water structure (Figure 5) remained similar. It was observed that the inclusion of the PE into the interfacial water structure through direct water bridging (Figure 6) is a key factor in determining binding affinity. More details on indirect water bridging are provided in the Supporting Information. In addition, the long-range electrostatic potential profile (Figure 4) may aid in the adsorption of charged polymers.

In an experimental setting, the difference in adsorption affinity between ionized and neutral PAA chains may not be as pronounced as reported in our study. A growing crystalline face will facilitate a dynamic exchange of Ca^{2+} ions at the interface, which can be chelated by the PAA chains. The chelation of Ca^{2+} ions by ionized PAA chains could reduce the chain adsorption affinity, weakening the electrostatic interactions between the PAA chains and the surface. In addition, other PE chemistries, as well as copolymers of charged and uncharged monomers, may yield additional insights into the interplay between electrostatic and chemical effects on polymer adsorption.

The unique surface morphology of the calcite $(10\bar{1}4)$ surface, where CO_3^{2-} groups dominate the surface interactions, may also contribute to the observed adsorption behavior. The surface Ca^{2+} ions are partially hidden by the rotated CO_3^{2-} groups, which may favor the indirect bridging of the PAA chains through the interfacial water layer over direct binding to the surface Ca^{2+} ions. Future research should investigate the adsorption of PAA on multiple surfaces of the various

https://doi.org/10.1021/acs.langmuir.4c03301
Langmuir 2024, 40, 25931−25939

polymorphs of $CaCO_3$ to understand the full scope of PAA adsorption on $CaCO_3$ surfaces, as multiple surfaces are present in a crystalline $CaCO_3$ particle growing in solution.[36] The Ca^{2+}-terminated calcite basal plane, for example, may facilitate direct binding of PAA chains to the surface Ca^{2+} ions, which may lead to important differences in the binding affinity and selectivity of PAA chains to different $CaCO_3$ surfaces.

■ ASSOCIATED CONTENT

Supporting Information

The Supporting Information is available free of charge at https://pubs.acs.org/doi/10.1021/acs.langmuir.4c03301.

GROMACS and PLUMED input files for the simulations described in this paper are available at https://github.com/alec-glisman/Simulation-Two-Chain-PAA. Additional analysis scripts are available at https://github.com/alec-glisman/Analysis-Polyelectrolyte-Surface-Adsorption. Further details on the simulation methods and analyses: polymer radius of gyration profile near the calcite surface, relative density profiles of Na^+, Ca^{2+}, and Cl^- ions near the calcite surface, charge density profiles near the calcite surface, and distribution of binding modes of the polyelectrolyte to the calcite surface (PDF)

■ AUTHOR INFORMATION

Corresponding Author

Zhen-Gang Wang − *Division of Chemistry and Chemical Engineering, California Institute of Technology, Pasadena, California 91125, United States;* orcid.org/0000-0002-3361-6114; Email: zgw@caltech.edu

Authors

Alec Glisman − *Division of Chemistry and Chemical Engineering, California Institute of Technology, Pasadena, California 91125, United States;* orcid.org/0000-0001-9677-1958

Sriteja Mantha − *Division of Chemistry and Chemical Engineering, California Institute of Technology, Pasadena, California 91125, United States;* orcid.org/0000-0001-7813-0903

Decai Yu − *The Dow Chemical Company, Midland, Michigan 48674, United States*

Eric Paul Wasserman − *The Dow Chemical Company, Consumer Solutions R&D, Collegeville, Pennsylvania 19426, United States*

Scott Backer − *The Dow Chemical Company, Consumer Solutions R&D, Collegeville, Pennsylvania 19426, United States;* orcid.org/0000-0001-8595-0547

Larisa Reyes − *The Dow Chemical Company, Industrial Solutions R&D, Lake Jackson, Texas 77566, United States*

Complete contact information is available at: https://pubs.acs.org/10.1021/acs.langmuir.4c03301

Notes

The authors declare no competing financial interest.

■ ACKNOWLEDGMENTS

This work was supported by the Dow Chemical Company through a University Partnership Initiative grant. We benefited greatly from the discussions with our Dow collaborator, Dr. Thomas Kalantar. We thank Professor William Goddard, Dr. Tridip Das, Jihoon Oh, and Kayla H. Panora for their helpful discussions.

■ REFERENCES

(1) Weiner, S.; Addadi, L. Design strategies in mineralized biological materials. *J. Mater. Chem.* **1997**, *7*, 689−702.

(2) Simkiss, K.; Wilbur, K. M. *Biomineralization*; Elsevier, 2012.

(3) Dhami, N. K.; Reddy, M. S.; Mukherjee, A. Biomineralization of calcium carbonates and their engineered applications: A review. *Front. Microbiol.* **2013**, *4*, 314.

(4) Kocot, K. M.; Aguilera, F.; McDougall, C.; Jackson, D. J.; Degnan, B. M. Sea shell diversity and rapidly evolving secretomes: Insights into the evolution of biomineralization. *Front. Zool.* **2016**, *13*, 23.

(5) De Leeuw, N. H. Molecular dynamics simulations of the growth inhibiting effect of Fe^{2+}, Mg^{2+}, Cd^{2+}, and Sr^{2+} on calcite crystal growth. *J. Phys. Chem. B* **2002**, *106*, 5241−5249.

(6) Jung, G. Y.; Shin, E.; Park, J. H.; Choi, B. Y.; Lee, S. W.; Kwak, S. K. Thermodynamic Control of Amorphous Precursor Phases for Calcium Carbonate via Additive Ions. *Chem. Mater.* **2019**, *31*, 7547−7557.

(7) Sun, W.; Jayaraman, S.; Chen, W.; Persson, K. A.; Ceder, G. Nucleation of metastable aragonite CaCO3 in seawater. *Proc. Natl. Acad. Sci. U.S.A.* **2015**, *112*, 3199−3204.

(8) Feng, Q.; Pu, G.; Pei, Y.; Cui, F.; Li, H.; Kim, T. Polymorph and morphology of calcium carbonate crystals induced by proteins extracted from mollusk shell. *J. Cryst. Growth* **2000**, *216*, 459−465.

(9) Sikirić, M. D.; Füredi-Milhofer, H. The influence of surface active molecules on the crystallization of biominerals in solution. *Adv. Colloid Interface Sci.* **2006**, *128*−*130*, 135−158.

(10) Qasem, N. A.; Mohammed, R. H.; Lawal, D. U. Removal of heavy metal ions from wastewater: A comprehensive and critical review. *npj Clean Water* **2021**, *4*, 36.

(11) Amjad, Z.; Zuhl, R. W.; Zibrida, J. F. *Factors Influencing the Precipitation of Calcium-Inhibitor Salts in Industrial Water Systems Carbosperse K-700 Water Treatment Polymers*, 2003; Vol. *17*.

(12) Reddy, M. M.; Hoch, A. R. Calcite crystal growth rate inhibition by polycarboxylic acids. *J. Colloid Interface Sci.* **2001**, *235*, 365−370.

(13) Gebauer, D.; Cölfen, H.; Verch, A.; Antonietti, M. The Multiple Roles of Additives in CaCO3 Crystallization: A Quantitative Case Study. *Adv. Mater.* **2009**, *21*, 435−439.

(14) Kim, I. W.; Robertson, R. E.; Zand, R. Effects of some nonionic polymeric additives on the crystallization of calcium carbonate. *Cryst. Growth Des.* **2005**, *5*, 513−522.

(15) Picker, A.; Kellermeier, M.; Seto, J.; Gebauer, D.; Cölfen, H. The multiple effects of amino acids on the early stages of calcium carbonate crystallization. *Z. Kristallogr. Cryst. Mater.* **2012**, *227*, 744−757.

(16) Deng, H.; Shen, X. C.; Wang, X. M.; Du, C. Calcium carbonate crystallization controlled by functional groups: A mini-review. *Front. Mater. Sci.* **2013**, *7*, 62−68.

(17) Jafar Mazumder, M. A. A review of green scale inhibitors: Process, types, mechanism and properties. *Coatings* **2020**, *10*, 928−929.

(18) Huang, S.-C.; Naka, K.; Chujo, Y. A carbonate controlled-addition method for amorphous calcium carbonate spheres stabilized by poly (acrylic acid)s. *Langmuir* **2007**, *23*, 12086−12095.

(19) Huang, S.-C.; Naka, K.; Chujo, Y. Effect of molecular weights of poly (acrylic acid) on crystallization of calcium carbonate by the delayed addition method. *Polym. J.* **2008**, *40*, 154−162.

(20) Ouhenia, S.; Chateigner, D.; Belkhir, M.; Guilmeau, E.; Krauss, C. Synthesis of calcium carbonate polymorphs in the presence of polyacrylic acid. *J. Cryst. Growth* **2008**, *310*, 2832−2841.

(21) Gower, L.; Tirrell, D. Calcium carbonate films and helices grown in solutions of poly(aspartate). *J. Cryst. Growth* **1998**, *191*, 153−160.

(22) Aschauer, U.; Ebert, J.; Aimable, A.; Bowen, P. Growth modification of seeded calcite by carboxylic acid oligomers and

polymers: toward an understanding of complex growth mechanisms. *Cryst. Growth Des.* **2010**, *10*, 3956−3963.
(23) Schuitemaker, A.; Raiteri, P.; Demichelis, R. The atomic structure and dynamics at the $CaCO_3$ vaterite−water interface: A classical molecular dynamics study. *J. Chem. Phys.* **2021**, *154*, 164504.
(24) Raiteri, P.; Gale, J. D.; Quigley, D.; Rodger, P. M. Derivation of an Accurate Force-Field for Simulating the Growth of Calcium Carbonate from Aqueous Solution: A New Model for the Calcite−Water Interface. *J. Phys. Chem. C* **2010**, *114*, 5997−6010.
(25) Raiteri, P.; Demichelis, R.; Gale, J. D. Thermodynamically Consistent Force Field for Molecular Dynamics Simulations of Alkaline-Earth Carbonates and Their Aqueous Speciation. *J. Phys. Chem. C* **2015**, *119*, 24447−24458.
(26) Fenter, P.; Kerisit, S.; Raiteri, P.; Gale, J. D. Is the Calcite−Water Interface Understood? Direct Comparisons of Molecular Dynamics Simulations with Specular X-ray Reflectivity Data. *J. Phys. Chem. C* **2013**, *117*, 5028−5042.
(27) Liu, Z.; Wang, N.; Li, Y.; Li, X.; Shi, D.; He, W.; Wang, X.; Sun, W.; Lu, G. Charge-modulated calcite surface for anionic surfactant adsorption from molecular dynamics simulations. *Surface. Interfac.* **2022**, *33*, 102234.
(28) Chun, B. J.; Lee, S. G.; Choi, J. I.; Jang, S. S. Adsorption of carboxylate on calcium carbonate (10 1 4) surface: Molecular simulation approach. *Colloids Surf., A* **2015**, *474*, 9−17.
(29) Aschauer, U.; Spagnoli, D.; Bowen, P.; Parker, S. C. Growth modification of seeded calcite using carboxylic acids: Atomistic simulations. *J. Colloid Interface Sci.* **2010**, *346*, 226−231.
(30) Sparks, D. J.; Romero-González, M. E.; El-Taboni, E.; Freeman, C. L.; Hall, S. A.; Kakonyi, G.; Swanson, L.; Banwart, S. A.; Harding, J. H. Adsorption of poly acrylic acid onto the surface of calcite: An experimental and simulation study (SUPPLEMENTAL). *Phys. Chem. Chem. Phys.* **2015**, *17*, 27357−27365.
(31) Zhu, B.; Xu, X.; Tang, R. Hydration layer structures on calcite facets and their roles in selective adsorptions of biomolecules: A molecular dynamics study. *J. Chem. Phys.* **2013**, *139*, 234705.
(32) Poudel, L.; Tamerler, C.; Misra, A.; Ching, W.-Y. Atomic-scale quantification of interfacial binding between peptides and inorganic crystals: The case of calcium carbonate binding peptide on aragonite. *J. Phys. Chem. C* **2017**, *121*, 28354−28363.
(33) Xue, Z.; Shen, Q.; Liang, L.; Shen, J.-W.; Wang, Q. Adsorption behavior and mechanism of SCA-1 on a calcite surface: A molecular dynamics study. *Langmuir* **2017**, *33*, 11321−11331.
(34) Mantha, S.; Glisman, A.; Yu, D.; Wasserman, E. P.; Backer, S.; Wang, Z.-G. Adsorption isotherm and mechanism of Ca^{2+} binding to polyelectrolyte. *Langmuir* **2024**, *40*, 6212−6219.
(35) Glisman, A.; Mantha, S.; Yu, D.; Wasserman, E. P.; Backer, S.; Wang, Z.-G. Multi-valent ion-mediated polyelectrolyte association and structure. *Macromolecules* **2024**, *57*, 1941−1949.
(36) De Leeuw, N. H.; Parker, S. C. Surface Structure and Morphology of Calcium Carbonate Polymorphs Calcite, Aragonite, and Vaterite: An Atomistic Approach. *J. Phys. Chem. B* **1998**, *102*, 2914−2922.
(37) Jo, S.; Kim, T.; Iyer, V. G.; Im, W. CHARMM-GUI A web-based graphical user interface for CHARMM. *J. Comput. Chem.* **2008**, *29*, 1859−1865.
(38) Choi, Y. K.; Park, S.-J.; Park, S.; Kim, S.; Kern, N. R.; Lee, J.; Im, W. CHARMM-GUI polymer builder for modeling and simulation of synthetic polymers. *J. Chem. Theory Comput.* **2021**, *17*, 2431−2443.
(39) Downs, R. T.; Hall-Wallace, M. The American Mineralogist crystal structure database. *Am. Mineral.* **2003**, *88*, 247−250.
(40) Markgraf, S. A.; Reeder, R. J. High-temperature structure refinements of calcite and magnesite. *Am. Mineral.* **1985**, *70*, 590−600.
(41) Ong, S. P.; Richards, W. D.; Jain, A.; Hautier, G.; Kocher, M.; Cholia, S.; Gunter, D.; Chevrier, V. L.; Persson, K. A.; Ceder, G. Python Materials Genomics (pymatgen): A robust, open-source python library for materials analysis. *Comput. Mater. Sci.* **2013**, *68*, 314−319.
(42) Berendsen, H. J.; van der Spoel, D.; van Drunen, R. GROMACS: A message-passing parallel molecular dynamics implementation. *Comput. Phys. Commun.* **1995**, *91*, 43−56.
(43) Van Der Spoel, D.; Lindahl, E.; Hess, B.; Groenhof, G.; Mark, A. E.; Berendsen, H. J. GROMACS: Fast, flexible, and free. *J. Comput. Chem.* **2005**, *26*, 1701−1718.
(44) Abraham, M. J.; Murtola, T.; Schulz, R.; Páll, S.; Smith, J. C.; Hess, B.; Lindahl, E. GROMACS: High performance molecular simulations through multi-level parallelism from laptops to supercomputers. *SoftwareX* **2015**, *1*, 19−25.
(45) Berendsen, H. J.; Grigera, J. R.; Straatsma, T. P. The missing term in effective pair potentials. *J. Phys. Chem.* **1987**, *91*, 6269−6271.
(46) Wang, J.; Wolf, R. M.; Caldwell, J. W.; Kollman, P. A.; Case, D. A. Development and testing of a general amber force field. *J. Comput. Chem.* **2004**, *25*, 1157−1174.
(47) Wang, J.; Wang, W.; Kollman, P. A.; Case, D. A. Automatic atom type and bond type perception in molecular mechanical calculations. *J. Mol. Graph. Model.* **2006**, *25*, 247−260.
(48) Sprenger, K.; Jaeger, V. W.; Pfaendtner, J. The general AMBER force field (GAFF) can accurately predict thermodynamic and transport properties of many ionic liquids. *J. Phys. Chem. B* **2015**, *119*, 5882−5895.
(49) Leontyev, I. V.; Stuchebrukhov, A. A. Electronic continuum model for molecular dynamics simulations. *J. Chem. Phys.* **2009**, *130*, 085102.
(50) Duboué-Dijon, E.; Javanainen, M.; Delcroix, P.; Jungwirth, P.; Martinez-Seara, H. A practical guide to biologically relevant molecular simulations with charge scaling for electronic polarization. *J. Chem. Phys.* **2020**, *153*, 050901.
(51) Bonomi, M.; Branduardi, D.; Bussi, G.; Camilloni, C.; Provasi, D.; Raiteri, P.; Donadio, D.; Marinelli, F.; Pietrucci, F.; Broglia, R. A.; et al. PLUMED: A portable plugin for free-energy calculations with molecular dynamics. *Comput. Phys. Commun.* **2009**, *180*, 1961−1972.
(52) Tribello, G. A.; Bonomi, M.; Branduardi, D.; Camilloni, C.; Bussi, G. PLUMED 2: New feathers for an old bird. *Comput. Phys. Commun.* **2014**, *185*, 604−613.
(53) Bussi, G.; Camilloni, C.; Tribello, G. A.; Banáš, P.; Barducci, A.; Bernetti, M.; Bolhuis, P. G.; Bottaro, S.; Branduardi, D.; The PLUMED consortium. Promoting transparency and reproducibility in enhanced molecular simulations. *Nat. Methods* **2019**, *16*, 670−673.
(54) Darden, T.; York, D.; Pedersen, L. Particle mesh Ewald: An N log (N) method for Ewald sums in large systems. *J. Chem. Phys.* **1993**, *98*, 10089−10092.
(55) Essmann, U.; Perera, L.; Berkowitz, M. L.; Darden, T.; Lee, H.; Pedersen, L. G. A smooth particle mesh Ewald method. *J. Chem. Phys.* **1995**, *103*, 8577−8593.
(56) Hess, B.; Bekker, H.; Berendsen, H. J.; Fraaije, J. G. LINCS: A linear constraint solver for molecular simulations. *J. Comput. Chem.* **1997**, *18*, 1463−1472.
(57) Nosé, S. A unified formulation of the constant temperature molecular dynamics methods. *J. Chem. Phys.* **1984**, *81*, 511−519.
(58) Hoover, W. G. Canonical dynamics: Equilibrium phase-space distributions. *Phys. Rev. A:At., Mol., Opt. Phys.* **1985**, *31*, 1695.
(59) Parrinello, M.; Rahman, A. Polymorphic transitions in single crystals: A new molecular dynamics method. *J. Appl. Phys.* **1981**, *52*, 7182−7190.
(60) Levine, Z. A.; Fischer, S. A.; Shea, J.-E.; Pfaendtner, J. Trp-cage folding on organic surfaces. *J. Phys. Chem. B* **2015**, *119*, 10417−10425.
(61) Ferreira, E. S.; Pereira, C. M.; Cordeiro, M. N. D.; dos Santos, D. J. Molecular dynamics study of the gold/ionic liquids interface. *J. Phys. Chem. B* **2015**, *119*, 9883−9892.
(62) Invernizzi, M.; Parrinello, M. Rethinking Metadynamics: From Bias Potentials to Probability Distributions. *J. Phys. Chem. Lett.* **2020**, *11*, 2731−2736.
(63) Rizzi, V.; Aureli, S.; Ansari, N.; Gervasio, F. L. OneOPES, a Combined Enhanced Sampling Method to Rule Them All. *J. Chem. Theory Comput.* **2023**, *19*, 5731−5742.

https://doi.org/10.1021/acs.langmuir.4c03301
Langmuir 2024, 40, 25931−25939

(64) Invernizzi, M.; Parrinello, M. Exploration vs Convergence Speed in Adaptive-Bias Enhanced Sampling. *J. Chem. Theory Comput.* **2022**, *18*, 3988−3996.
(65) Invernizzi, M.; Piaggi, P. M.; Parrinello, M. Unified approach to enhanced sampling. *Phys. Rev. X* **2020**, *10*, 041034.

https://doi.org/10.1021/acs.langmuir.4c03301
Langmuir 2024, 40, 25931−25939